

A dispersive effective equation for transverse propagation of planar shallow water waves over periodic bathymetry

David I. Ketcheson* Giovanni Russo†

September 4, 2024

Abstract

We study the behavior of shallow water waves propagating over bathymetry that varies periodically in one direction and is constant in the other. Plane waves traveling along the constant direction are known to evolve into solitary waves, due to an effective dispersion. We apply multiple-scale perturbation theory to derive an effective constant-coefficient system of Boussinesq-type equations that not only accurately describe these waves but also predict their full two-dimensional shape in some detail. Numerical experiments confirm the good agreement between the effective equations and the variable-bathymetry shallow water equations.

1 Model Equations and Assumptions

In this work we study the shallow water wave (or Saint-Venant) model:

$$h_t + (hu)_x + (hv)_y = 0 \quad (1a)$$

$$(hu)_t + \left(hu^2 + \frac{1}{2}gh^2 \right)_x + (huv)_y = -ghb_x \quad (1b)$$

$$(hv)_t + \left(hv^2 + \frac{1}{2}gh^2 \right)_y + (huv)_x = -ghb_y \quad (1c)$$

where $g = 9.81$ is the gravitational acceleration, $h(x, y, t)$ denotes the depth, $u(x, y, t), v(x, y, t)$ the horizontal velocity components, and $b(x, y)$ the bottom elevation (bathymetry). We are interested in the behavior of waves propagating over bathymetry that does not depend on x , and is periodic in y with period δ :

$$b(y + \delta) = b(y),$$

focusing on propagation of initially-planar waves traveling parallel to the x -axis:

$$\eta(x, y, 0) = \eta_0(x) \quad u(x, y, 0) = u_0(x) \quad v(x, y, 0) = 0. \quad (2)$$

Here $\eta = h + b$ is the surface elevation. Due to symmetry, this can equivalently be seen as a model for waves in a non-rectangular channel with frictionless walls [10, Section 1.2], a problem which has also been studied (using other water wave models) for instance in [8, 11, 2].

It has been shown that linear plane waves traveling parallel to variations in the medium of propagation exhibit effective dispersion if there is variation in the sound speed [9]. For nonlinear shallow water waves this effective dispersion can lead to the formation of solitary waves even though the equations themselves are non-dispersive [10]. In the latter work, a partially-heuristic constant-coefficient KdV-type model was shown to approximate the behavior of such waves. We refer also to [2] for development of a similar model and comparison with experiments. In the present work we develop a more accurate and detailed effective model for these waves. We apply multiple-scale perturbation analysis to show that these waves are described, to leading order, by a Boussinesq-type system with dispersive coefficient depending on the

*david.ketcheson@kaust.edu.sa, Applied Mathematics and Computational Science, CEMSE Division, King Abdullah University of Science and Technology (KAUST), Thuwal, 23955-6900, Kingdom of Saudi Arabia

†giovanni.russo@unict.it, Department of Mathematics and Computer Science, University of Catania, Viale A. Doria 6, 95125 Catania, Italy

bathymetry. The effective model describes the full two-dimensional structure of the waves, and is shown to be in agreement with detailed numerical simulations.

The perturbation approach used here is based on that developed by Yong and coauthors [12, 6]. We have conducted a similar analysis for plane waves propagating perpendicular to the bathymetric variation; in that case the problem can be reduced to one horizontal dimension [4]. In the one-dimensional setting, effective dispersion is caused by wave reflection, whereas in the setting of the present work it is caused by propagation perpendicular to the direction of propagation of the wave itself and may be described as the result of refraction or diffraction [9].

Throughout the paper we use dimensional quantities with SI units, so lengths are measured in meters and time in seconds.

The rest of the paper is organized as follows. In Section 2 we perform a multiple-scale analysis leading to an effective medium equation for the waves of interest; the main result is equation (22), which describes the evolution of such waves after averaging over the y -dimension. In Section 3 we compare solutions of the effective equations with those of the original variable-bathymetry system (1). In Section (4) we investigate the shape of these two-dimensional solitary waves, comparing the predictions of the multiple-scale analysis with the results of numerical experiments. Some conclusions are provided in Section 5.

2 Multiple-Scale Analysis

The choice of primary variables is a key decision in perturbation analysis of systems like the one considered here. One usually works with the conserved variables (h, hu, hv) in order to include weak solutions, but here we are interested in strong solutions. Since we seek to derive a system of equations describe the variation of the solution over long length scales, we prefer to use quantities that do not necessarily vary on the periodic microscale for near-equilibrium solutions (see e.g. [6, 4] for other examples). In the present setting this indicates that one should use the surface elevation η rather than h and the y -momentum $p = hv$ rather than v . After some trial and error we found it best to rewrite (1) in terms of (η, u, p) :

$$\eta_t + (u(\eta - b))_x + p_y = 0 \quad (3a)$$

$$u_t + uu_x + g\eta_x + \frac{p}{\eta - b}u_y = 0 \quad (3b)$$

$$p_t + \left(\frac{p^2}{\eta - b} \right)_y + g(\eta - b)\eta_y + (pu)_x = 0. \quad (3c)$$

Note that it is not important to write the equations in conservation form since we are primarily interested in strong solutions of this system.

A second critical choice is that of a small parameter. We assume that the wavelength of the typical waves we are interested in is long relative to the period δ of the bathymetry. We perform a change of variables, by introducing $\tilde{y} = y/\delta$, so now $b(y) = b(\tilde{y}\delta) = \tilde{b}(\tilde{y})$, with \tilde{b} a 1-periodic function, and $\partial/\partial y = \delta^{-1}\partial/\partial\tilde{y}$. We next rewrite the equations in the new coordinates (x, \tilde{y}, t) and suppress the tildes to obtain

$$\eta_t + (u(\eta - b))_x + \delta^{-1}p_y = 0 \quad (4a)$$

$$u_t + uu_x + g\eta_x + \delta^{-1}\frac{p}{\eta - b}u_y = 0 \quad (4b)$$

$$p_t + \delta^{-1}\left(\frac{p^2}{\eta - b} \right)_y + \delta^{-1}g(\eta - b)\eta_y + (pu)_x = 0. \quad (4c)$$

We now look for solutions which are small perturbations, of $O(\delta)$, of the lake at rest given by $(\eta, u, p) = (\eta_0, 0, 0)$.

We assume the quantities η, u, p can be written as power series in δ with the form

$$\eta - \eta^0 = \delta\eta^1(x, y, t) + \delta^2\eta^2(x, y, t) + \dots \quad (5a)$$

$$u = \delta u^1(x, y, t) + \delta^2 u^2(x, y, t) + \dots \quad (5b)$$

$$p = \delta p^1(x, y, t) + \delta^2 p^2(x, y, t) + \dots \quad (5c)$$

Here and throughout this section, superscripts on η, u , and p denote indices of the asymptotic expansion (5). When needed, we shall adopt parentheses to denote exponentiation of these quantities. All functions

are assumed to be periodic in y . In what follows, we use $\langle \cdot \rangle$ to denote quantities that are averaged with respect to y , i.e. for any function $f(x, y, t)$ we have

$$\langle f \rangle = \int_0^1 f dy.$$

Notice that if f does not depend on y then $f = \langle f \rangle$, and that $\langle \cdot \rangle$ commutes with x and t derivatives, i.e. $\langle f \rangle_t = \langle f_t \rangle$ and $\langle f \rangle_x = \langle f_x \rangle$. Throughout the paper we denote by $H(y) \equiv \eta^0 - b(y)$ the unperturbed water depth.

Next, we substitute (5) into (4) and equate terms at each power of δ .

2.1 $\mathcal{O}(\delta^0)$

First we collect all terms proportional to δ^0 . The expansion of (4b) does not contain any such terms. From the expansion of (4a) we obtain $p_y^1 = 0$ while (4c) gives

$$gH(y)\eta_y^1 = 0$$

From these relations we deduce that p^1 and η^1 do not depend on y .

2.2 $\mathcal{O}(\delta^1)$

Next, collecting terms proportional to δ^1 , we obtain

$$\eta_t^1 + Hu_x^1 + p_y^2 = 0 \tag{6a}$$

$$u_t^1 + g\eta_x^1 = 0 \tag{6b}$$

$$p_t^1 - \frac{(p^1)^2}{H^2} H'(y) + gH\eta_y^2 = 0, \tag{6c}$$

Now we average these equations with respect to y – i.e., we integrate (6) with respect to y over one period, noting that the average of any y -derivative is zero. Since η^1 is independent of y , Eq. (6b) implies that u_t^1 is also independent of y . Since we assume that $u(x, y, 0)$ is independent of y we deduce further that u^1 does not depend on y , so we obtain

$$\langle u_t^1 \rangle + g \langle \eta_x^1 \rangle = 0.$$

Solving (6c) for η_y^2 and averaging the result gives

$$-\frac{\langle H^{-1} \rangle}{g} \langle p_t^1 \rangle = 0.$$

Since we assume $p(x, y, 0) = 0$, this implies $p^1 = 0$. Returning to (6c), this in turn implies $\eta_y^2 = 0$, so $\eta^2 = \langle \eta^2 \rangle$. Averaging (6a) in y gives

$$\langle \eta_t^1 \rangle + \langle H \rangle \langle u_x^1 \rangle = 0. \tag{7}$$

Taking together these averaged equations, we have the system

$$\langle \eta_t^1 \rangle + \langle H \rangle \langle u_x^1 \rangle = 0 \tag{8a}$$

$$\langle u_t^1 \rangle + g \langle \eta_x^1 \rangle = 0, \tag{8b}$$

which is simply the linear wave equation with wave speed $c = \sqrt{g \langle H \rangle}$. It is interesting to note that here the average depth appears in the wave speed, whereas the harmonic average appears for waves propagating perpendicular to the lines of constant bathymetry (see [4], and also [9]).

We can further manipulate (6a) to obtain an expression for p^2 , the leading-order term in the y -momentum. Subtracting (8a) from (6a) we obtain

$$-p_y^2 = \{ \eta_t^1 \} + \{ H \} u_x^1$$

where, for any function f , we denote by

$$\{ f \} \equiv f - \langle f \rangle$$

the *fluctuating part* of f . Considering that $\eta^1 = \langle \eta^1 \rangle$ we have

$$p_y^2 = -\{H\} u_x^1$$

Taking the indefinite integral of this equation respect to y we obtain

$$\int_0^y p^2(x, s, t)_s ds = p^2(x, y, t) = -\llbracket H \rrbracket u_x^1 + \langle p^2 \rangle, \quad (9)$$

where $\llbracket f \rrbracket$ denotes the integral of the fluctuating part of f :

$$\llbracket f \rrbracket = \int_s^y (f(\xi) - \langle f \rangle) d\xi \quad \text{where } s \text{ is chosen so that } \langle \llbracket f \rrbracket \rangle = 0.$$

2.3 $\mathcal{O}(\delta^2)$

Collecting terms proportional to δ^2 , we obtain

$$-p_y^3 = \eta_t^2 + H u_x^2 + (\langle \eta^1 \rangle \langle u^1 \rangle)_x \quad (10a)$$

$$0 = u_t^2 + \langle u^1 \rangle \langle u_x^1 \rangle + g \langle \eta_x^2 \rangle \quad (10b)$$

$$-g \eta_y^3 = \frac{1}{H} (p_t^2 + g \langle \eta^1 \rangle \langle \eta_y^2 \rangle) = \frac{1}{H} (-\llbracket H \rrbracket \langle u_{xt}^1 \rangle + \langle p^2 \rangle_t). \quad (10c)$$

In the last line we have used that η^2 is independent of y and Equation (9). The only term in (10b) that could depend on y is u_t^2 , so it must be independent of y ; i.e. $u^2 = \langle u^2 \rangle(x, t)$. Thus we have

$$\langle u_t^2 \rangle + \langle u^1 \rangle \langle u_x^1 \rangle + g \langle \eta_x^2 \rangle = 0. \quad (11)$$

Taking the average of (10a) gives

$$\langle \eta_t^2 \rangle + \langle H \rangle \langle u_x^2 \rangle + (\langle \eta^1 \rangle \langle u^1 \rangle)_x = 0. \quad (12)$$

Subtracting this from (10a) and integrating in y , we get

$$p^3(x, y, t) = -\llbracket H \rrbracket \langle u_x^2 \rangle + \langle p^3 \rangle. \quad (13)$$

For simplicity we now specialize our analysis to bathymetry profiles for which $\langle H^{-1} \llbracket H \rrbracket \rangle = 0$, which holds for instance for piecewise-constant or sinusoidal bathymetry. Then taking the average of (10c), we find that $\langle p^2 \rangle_t = 0$. Since $p^2(x, y, 0) = 0$, it follows that $\langle p^2 \rangle = 0$. Then integrating (10c) in y yields

$$\eta^3(x, y, t) = \frac{1}{g} \llbracket H^{-1} \llbracket H \rrbracket \rrbracket \langle u_{xt}^1 \rangle + \langle \eta^3 \rangle. \quad (14)$$

Based on what we have determined up to this point, we can write the series (5) more simply as

$$\eta - \eta^0 = \delta \eta^1(x, t) + \delta^2 \eta^2(x, t) + \dots \quad (15a)$$

$$u = \delta u^1(x, t) + \delta^2 u^2(x, t) + \dots \quad (15b)$$

$$p = \delta^2 p^2(x, y, t) + \dots \quad (15c)$$

Let $\bar{\eta} = \delta^{-1} \langle \eta - \eta^0 \rangle$ and $\bar{u} = \delta^{-1} \langle u \rangle$. By adding δ times (8a) to δ^2 times (12), we get an approximate equation for the evolution of $\bar{\eta}$:

$$\delta (\bar{\eta}_t + \langle H \rangle \bar{u}_x) + \delta^2 (\bar{\eta} \bar{u})_x = \mathcal{O}(\delta^3). \quad (16a)$$

Similarly, by adding δ times (8b) to δ^2 times (11), we get an approximate equation for the evolution of \bar{u} :

$$\delta (\bar{u}_t + g \bar{\eta}_x) + \delta^2 (\bar{u} \bar{u}_x) = \mathcal{O}(\delta^3). \quad (16b)$$

We see that up to this order, the y -averaged variables satisfy a nonlinear first-order hyperbolic system. We proceed with the analysis at the next order, where we expect to see dispersive terms.

2.4 $\mathcal{O}(\delta^3)$

Collecting terms proportional to δ^3 , we obtain

$$\eta_t^3 + Hu_x^3 + (\eta^1 u^2 + \eta^2 u^1)_x = -p_y^4 \quad (17a)$$

$$u_t^3 + (u^1 u^2)_x + \llbracket H^{-1} \llbracket H \rrbracket \rrbracket u_{xtx}^1 + g\eta_x^3 = 0 \quad (17b)$$

$$\frac{1}{H} (p_t^3 - H^{-2}(p^2)^2 H' + 2H^{-1} p^2 p_y^2 + g\eta^1 \eta_y^3 + (p^2 u^1)_x) = -g\eta_y^4. \quad (17c)$$

Averaging (17a) yields

$$\langle \eta^3 \rangle_t + \langle Hu^3 \rangle_x + (\langle \eta^1 \rangle \langle u^2 \rangle + \langle \eta^2 \rangle \langle u^1 \rangle)_x = 0. \quad (18)$$

Since u^3 may depend on y , we must work directly with the average $\langle Hu^3 \rangle$. We therefore multiply (17b) by H before averaging, to obtain

$$\langle Hu^3 \rangle_t + \langle H \rangle (\langle u^1 \rangle \langle u^2 \rangle)_x - \mu \langle u_{xxt}^1 \rangle + g \langle H \rangle \langle \eta_x^3 \rangle = 0. \quad (19)$$

where

$$\mu = -\langle H \llbracket H^{-1} \llbracket H \rrbracket \rrbracket \rangle = \langle H^{-1} (\llbracket H \rrbracket)^2 \rangle. \quad (20)$$

The last equality comes from the general property $\llbracket a \llbracket b \rrbracket \rrbracket + \llbracket \llbracket a \rrbracket b \rrbracket = 0$ for all functions $a(y)$ $b(y)$ [12, Appendix A].

Introducing $\langle q^j \rangle = \langle Hu^j \rangle$, this is

$$\langle q^3 \rangle_t + \langle H \rangle^{-1} (\langle q^1 \rangle \langle q^2 \rangle)_x - \langle H \rangle^{-1} \mu \langle q_{xxt}^1 \rangle + g \langle H \rangle \langle \eta_x^3 \rangle = 0. \quad (21)$$

Averaging (17c), after a number of tedious calculations, yields $\langle p^3 \rangle = 0$.

2.5 Governing equations for averaged variables

Let $\bar{q} = \sum_j \delta^{j-1} \langle q^j \rangle$. We now add $\delta \langle H \rangle$ times (8b), plus $\delta^2 \langle H \rangle$ times (11), plus δ^3 times (21). This gives

$$\delta(\bar{q}_t + g \langle H \rangle \bar{\eta}_x) + \delta^2 \langle H \rangle^{-1} \bar{q} \bar{q}_x = \delta^3 \langle H \rangle^{-1} \mu \bar{q}_{xxt} + \mathcal{O}(\delta^4) \quad (22a)$$

Similarly, adding δ times (8a) with δ^2 times (12) with δ^3 times (18) results in

$$\delta(\bar{\eta}_t + \bar{q}_x) + \delta^2 \langle H \rangle^{-1} (\bar{\eta} \bar{q})_x = \mathcal{O}(\delta^4). \quad (22b)$$

In the special case that $g = \langle H \rangle = 1$ and $\mu = 1/3$, this system is referred to as the classical Boussinesq system. It is known to be well-posed [1, Thm. 3.3].

3 Numerical comparison

In this section we explore the accuracy of the homogenized approximation by comparing its numerical solutions to numerical solutions of the original system (1). We start by discussing the methods adopted for the numerical solution of both the original system (1) and the homogenized system (22).

3.1 Numerical discretization of the homogenized equations

We solve the homogenized equations (22) with a Fourier pseudospectral discretization in space and explicit 3-stage 3rd-order SSP Runge-Kutta integration in time. We can write this system as

$$\bar{\eta}_t = -\bar{q}_x - \delta \langle H \rangle^{-1} (\bar{\eta} \bar{q})_x \quad (23)$$

$$\bar{q}_t = -(1 - \delta^2 \langle H \rangle^{-1} \mu \partial_x^2)^{-1} (g \langle H \rangle \bar{\eta}_x + \delta \langle H \rangle^{-1} \bar{q} \bar{q}_x) \quad (24)$$

We discretize in the standard pseudospectral way and then apply the inverse elliptic operator $(1 - \delta^2 \langle H \rangle^{-1} \mu \partial_x^2)^{-1}$ in Fourier space, which does not require the solution of any algebraic system. We can therefore integrate the pseudospectral semi-discretization of (23) efficiently with an explicit Runge–Kutta method.

For the spatial domain, we take $x \in [-L, L]$ where L is chosen large enough that the waves do not reach the boundaries before the final time.

3.2 Numerical methods for the variable-bathymetry shallow water system

For the solution of the first-order variable-coefficient hyperbolic shallow water system (1) we use two different approaches, depending on the nature of the bathymetry. Accurate solution of this system is much more expensive as it requires a much finer spatial mesh, in order to resolve the bathymetric variation and its effects, and it requires the solution of a problem in two space dimensions. applied at $x = 0$.

For piecewise-constant (discontinuous) bathymetry, we use the finite volume code Clawpack [5, 7], employing the *SharpClaw* algorithm, based on 5th-order WENO reconstruction in space and 4th-order Runge–Kutta integration in time [3]. This algorithm is well adapted to handle the lack of regularity in both the coefficients and the solution. For continuous bathymetry, we use a standard Fourier collocation pseudospectral method in space and 4th-order Runge–Kutta integration in time. Ordinarily one would avoid the use of spectral methods for a first-order hyperbolic problem, but since we focus on scenarios in which shocks do not form, this method performs well and is more efficient than a finite volume discretization, as long as the bathymetry is continuous.

3.3 Piecewise-constant bathymetry

We first consider the following setup:

$$b(x, y) = \begin{cases} -2/5 & 0 \leq y < 1/2 \\ -8/5 & 1/2 \leq y < 1 \end{cases} \quad (25a)$$

$$\eta(x, y, 0) = \frac{1}{20} \exp(-(x/5)^2) \quad (25b)$$

$$u(x, y, 0) = 0 \quad (25c)$$

$$v(x, y, 0) = 0 \quad (25d)$$

The problem domain is $(x, y) \in [-350, 350] \times [-1/2, 1/2]$ with periodic boundary conditions. The initial surface perturbation splits into a left-going and right-going pulse, each of which eventually resolves into a series of traveling waves. In order to save computational effort in the finite volume solution, we take the spatial domain $[0, L]$ with a reflecting (solid wall) boundary condition. In Figure 1 we show snapshots of the right-going pulse. We see extremely close agreement between the solutions, with some differences visible at late times, after the pulse has propagated for hundreds of meters. This scenario was chosen specifically to show agreement between the homogenized model and the original problem, by taking a relatively small initial perturbation.

3.4 Smooth bathymetry

Next we consider the smoothly-varying bathymetry

$$b = -1 + \frac{3}{10} \sin(2\pi y) \quad (26)$$

with the same initial data as in (25). Results are shown in Figure 2. Because the relatively smaller variation in bathymetry leads to a smaller effective dispersion, the initial pulse divides into a larger number of solitary waves. Again we see that the solution of the homogenized system agrees with that of the variable-coefficient system, with the discrepancy between the two growing over time.

In Figure 3 we plot the difference between the homogenized and variable-bathymetry solution (averaged) versus time. We see that after an initial phase, the error grows linearly, and seems primarily due to a growing phase error between the corresponding solitary waves in the two solutions.

4 Solitary wave shape

In this section we study the shape of the solitary waves observed in numerical simulations and compare them with predictions based on the homogenized equations. We first consider travelling wave solutions of the homogenized equations, and then investigate the full two-dimensional solitary waves in more detail.

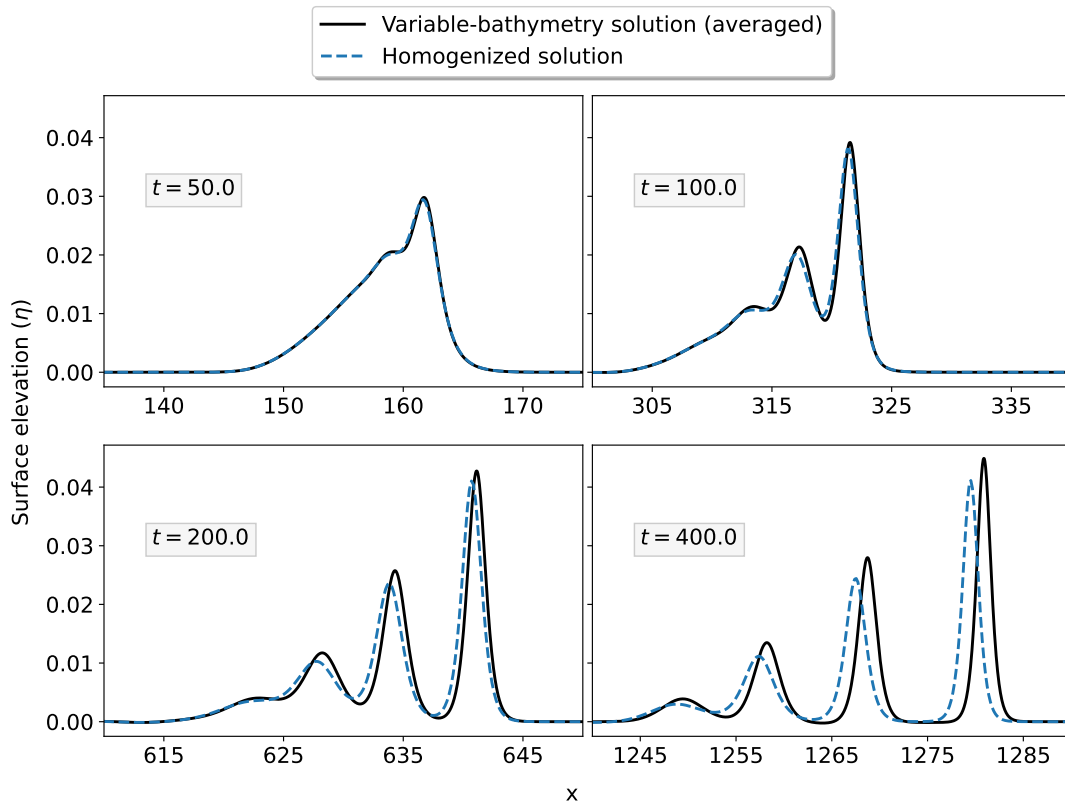


Figure 1: Comparison of homogenized and direct solutions, for piecewise-constant bathymetry (25). The surface elevation $\eta - \eta^0$ is shown.

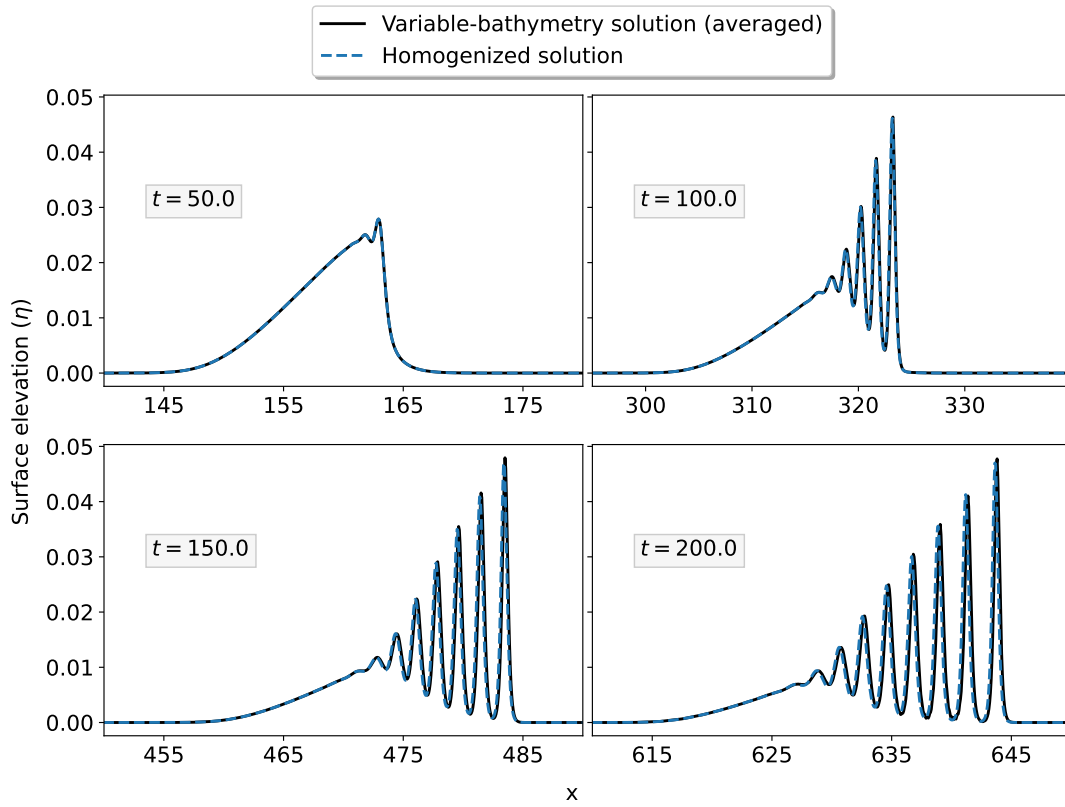


Figure 2: Comparison of homogenized and direct solutions, for sinusoidal bathymetry (26). The surface elevation $\eta - \eta^0$ is shown.

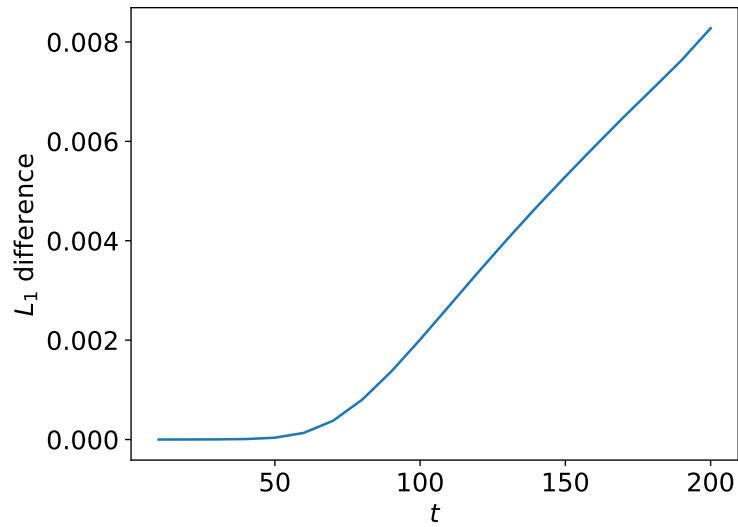


Figure 3: L_1 norm of difference between homogenized and averaged solution surface height over time, for sinusoidal bathymetry (26).

4.1 Traveling wave solutions of the homogenized equations

Now we consider the problem of finding the traveling wave solution for the homogenized system (22). Neglecting the higher order term, after dividing by δ , the system can be written in the form

$$q_t + a_1 \eta_x + a_2 q q_x - \tilde{\mu} q_{xxt} = 0 \quad (27)$$

$$\eta_t + q_x + a_2 (\eta q)_x = 0 \quad (28)$$

where we set $a_1 := g \langle H \rangle$, $a_2 := \delta \langle H \rangle$, $\tilde{\mu} := \delta^2 \mu / \langle H \rangle$. Now we look for traveling waves which depend only on $\xi = x - Vt$, propagating on a lake at rest, so that the unperturbed state is $q_0 = 0$, and, with a suitable choice of the frame of reference, $\eta_0 = 0$. Here V is the traveling speed of the wave. Assuming η and q are functions of ξ , we obtain that the wave has to satisfy the following set of ODEs:

$$-Vq' + a_1 \eta' + a_2 q q' + \tilde{\mu} V q''' = 0 \quad (29)$$

$$-V\eta' + q' + a_2 (\eta q)' = 0 \quad (30)$$

These equations can be written as

$$\frac{d}{d\xi} \left(-Vq + a_1 \eta + \frac{1}{2} a_2 q^2 + \tilde{\mu} V q'' \right) = 0 \quad (31)$$

$$\frac{d}{d\xi} (-V\eta + q + a_2 \eta q) = 0 \quad (32)$$

which gives

$$-Vq + a_1 \eta + \frac{1}{2} a_2 q^2 + \tilde{\mu} V q'' = C_1, \quad (33a)$$

$$-V\eta + q + a_2 \eta q = C_2. \quad (33b)$$

Since we assume the wave is a perturbation of the lake at rest with $\eta_0 = 0$, the two constants C_1 and C_2 are both zero. From the second equation we can express η as a function of q :

$$\eta = \frac{q}{V - a_2 q}.$$

Using this expression in (33a) we obtain the following ODE for $q(\xi)$:

$$q'' = \left(Vq - \frac{a_1 q}{V - a_2 q} - \frac{1}{2} a_2 q^2 \right) / (\tilde{\mu} V). \quad (34)$$

This equation is of the form

$$q'' = F(q),$$

so its dynamics is analogous to that of a particle with one degree of freedom, subject to an acceleration field which depends only on the position. Multiplying by q' and integrating we obtain

$$\frac{d}{d\xi} \left(\frac{1}{2} (q')^2 + U(q) \right) = 0$$

with $U(q) = -\int F(q) dq$ playing the role of the potential. Integrating the equation one gets the analogue of total energy conservation:

$$\frac{1}{2} (q')^2 + U(q) = E. \quad (35)$$

In this case the potential U is given by

$$U(q) = \left(\frac{1}{6} a_2 q^3 - \frac{1}{2} V q^2 - \frac{a_1}{a_2} - \frac{a_1}{a_2^2} V \log(1 - a_2 q / V) \right) / (\tilde{\mu} V)$$

The potential is defined up to an additive constant; we chose the constant in such a way that $U(0) = 0$. The trajectories of the material point in phase space (q, \dot{q}) are the lines which maintain constant total energy. Notice that if we approximate the log term by the first term in its expansion about $q = 0$, then the solution of (35) is a hyperbolic secant squared. Thus we expect that solitary waves will be close to this shape.

An example of potential, trajectories and traveling waves is illustrated in Figure 4. The first panel shows both the potential $U(q)$ corresponding to $V = 10/3$ (blue continuous line) and its best fit approximation with a cubic polynomial (magenta dashed line).

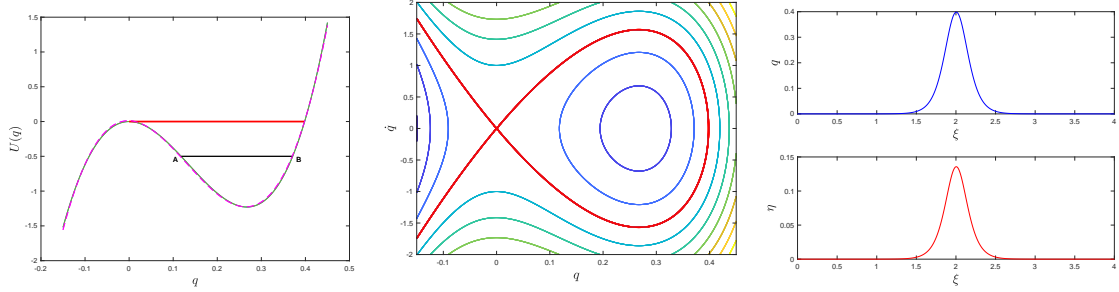


Figure 4: Construction of the traveling waves. Left panel: potential $U(q)$ corresponding to $V = 10/3$ (blue continuous line). If total energy and the particle is initially in the potential well, then the orbits are periodic (black line between points A and B). As the energy increases approaching zero from below, the period of the oscillations tends to infinity, and the trajectory becomes a traveling wave. Positive energy corresponds to open orbits. The central panel shows the lines with constant total energy corresponding to the same potential. The thick red line is the separatrix. The right panel is obtained by integrating the first order system for (q, q') , starting from a very small values aligned along the eigenvector of the linearized dynamical system corresponding to the positive eigenvalue.

4.2 Mean profile

First we consider the shape of the y -averaged surface. A typical y -averaged solution is shown in Figure 5a. As expected, these waves have a shape very close to the typical sech^2 , and seem to scale in the same way as other such solitons. In Figure 5b we plot each of the three tallest waves, after shifting the peak to be at $x = 0$ and rescaling the amplitude to 1 and rescaling the width by the square root of the amplitude. We see that the waves very nearly coincide with the reference sech^2 curve.

We have observed that much larger solitary waves have a more sharply-peaked shape; investigation of larger-amplitude solutions is the subject of ongoing work.

4.3 Full shape

Next we investigate the two-dimensional shape of these waves. For the bathymetry considered here, we have found that small-amplitude solitary wave solutions have the following shape:

$$\eta(x, y, t) - \eta^0 \approx f(x - ct; A) - \llbracket H^{-1} \llbracket H \rrbracket \rrbracket f''(x - ct; A) \quad (36a)$$

$$u(x, y, t) \approx \sqrt{g/\langle H \rangle} (\eta - \eta^0) \quad (36b)$$

$$p(x, y, t) \approx -\llbracket H \rrbracket \langle u_x \rangle, \quad (36c)$$

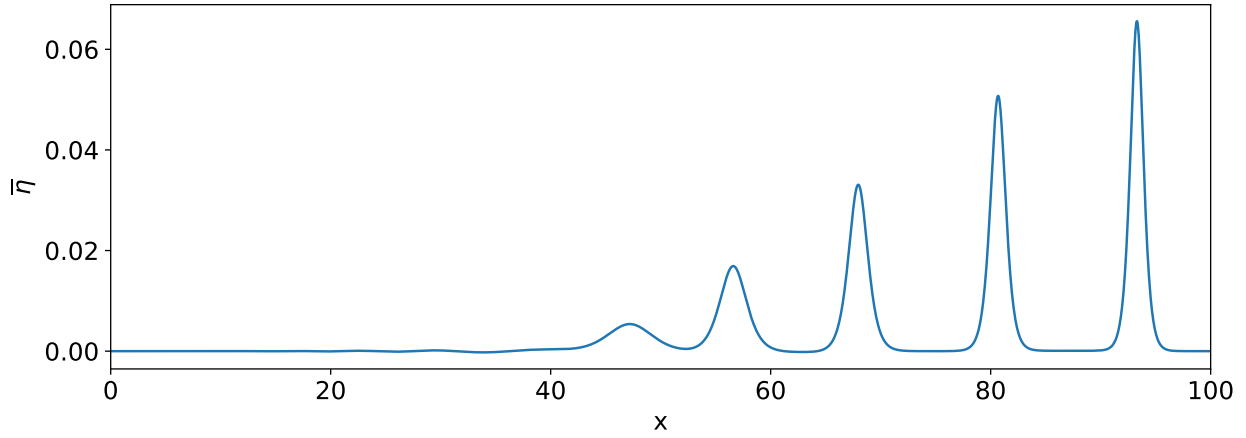
where

$$f(x; A) = A \text{sech}^2(\alpha \sqrt{A} x) \\ \alpha \approx 4.85$$

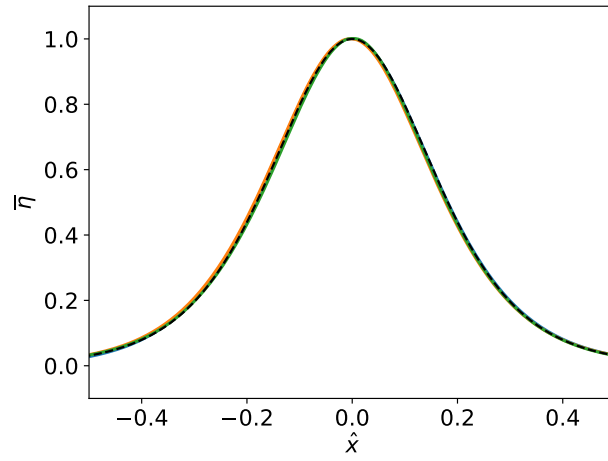
These properties can be anticipated based on the homogenization above. Relation (36b) holds for right-going waves in the solution of the lowest-order approximation (8), while (36c) is suggested by (9) and (13). The leading correction to the sech^2 shape, appearing in (36a), is suggested by (14).

In Figure 6a, we plot a numerical solitary wave versus the function (36a), for two slices in y . Similarly good agreement is seen for all values of y . Note that here, to fit the full two-dimensional solitary wave, we have used only the mean peak amplitude as a fitting parameter. Thus the waves we observe seem to belong to a one-parameter family.

Similar investigation of solitary waves over other bathymetric profiles (including smooth sinusoidal bathymetry) show that the waves have, to very good approximation, the shape prescribed in (36), with only the value of α varying depending on the bathymetry.

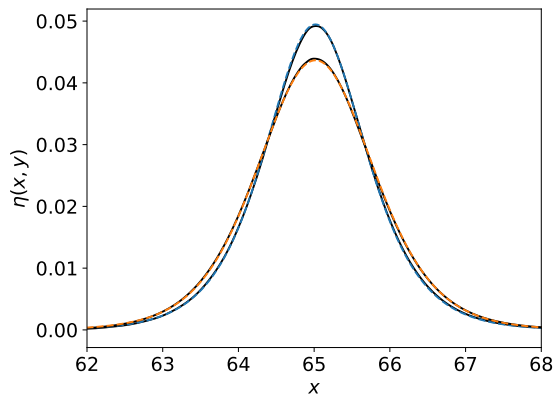


(a) Mean surface height versus x for a train of solitary waves.

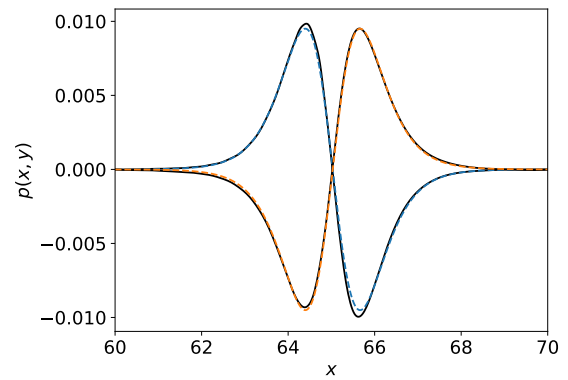


(b) Largest 3 waves rescaled and compared with a fitted sech^2 curve.

Figure 5: The mean surface height for small-amplitude solitary waves (solid lines) is very close to sech^2 (dashed line), and the waves' width scales inversely with the square root of the amplitude.



(a) Computed surface height versus x compared to (36a), for two values of y .



(b) Computed y -momentum (p) versus x compared to (36c), for two values of y .

Figure 6: Comparison of solitary wave shape with the formulas (36).

5 Conclusion

We have studied the behavior of initially-planar shallow water waves over a bottom that varies periodically in the transverse direction. These waves are described to good accuracy by the effective Boussinesq system (22), and exhibit the formation of solitary waves. Unlike solitary wave solutions of one-dimensional hyperbolic systems with periodic coefficients [6, 4], these are true traveling waves. The shape of small-amplitude solitary waves is close to one that can be expressed simply in terms of elementary functions, and is predicted by the equations obtained in the process of deriving the effective Boussinesq system.

Since water waves are naturally dispersive (even over a flat bottom), it is natural to ask about the behavior of water waves over periodic bathymetry when both natural dispersion and bathymetric dispersion are accounted for. This has been studied to some extent in [2, 10]; a full analysis starting from a dispersive water wave model is the subject of future work, and seems to require techniques beyond what we have used herein.

Many other questions about the behavior of these waves remain open. For instance, large-amplitude solitary waves have a different shape, and sufficiently large initial data leads to wave breaking, but the behavior of waves near the boundary between the dispersion-dominated and nonlinearity-dominated regime is complicated. The interaction of colliding solitary waves and the behavior of periodic traveling waves in this system are also of interest. Finally, a more thorough and careful characterization of the accuracy of the effective medium description would be of great interest.

Acknowledgment

This work was supported by funding from King Abdullah University of Science and Technology (KAUST). It was carried out in large part while the second author was a visiting professor at KAUST.

References

- [1] Jerry Lloyd Bona, Min Chen, and Jean-Claud Saut. Boussinesq equations and other systems for small-amplitude long waves in nonlinear dispersive media: II. the nonlinear theory. *Nonlinearity*, 17(3):925, 2004.
- [2] Rémi Chassagne, Andrea Gilberto Filippini, Mario Ricchiuto, and Philippe Bonneton. Dispersive and dispersive-like bores in channels with sloping banks. *Journal of Fluid Mechanics*, 870:595–616, 2019.
- [3] D. I. Ketcheson, M. Parsani, and R. J. LeVeque. High-order Wave Propagation Algorithms for Hyperbolic Systems. *SIAM Journal on Scientific Computing*, 35(1):A351–A377, 2013.
- [4] David I Ketcheson, Lajos Lóczi, and Giovanni Russo. A multiscale model for weakly nonlinear shallow water waves over periodic bathymetry. *arXiv preprint arXiv:2311.02603*, 2023.
- [5] R. J. LeVeque. *Finite Volume Methods for Hyperbolic Problems*. Cambridge University Press, 2002.
- [6] Randall J. LeVeque, Yong, and H. Darryl. Solitary waves in layered nonlinear media. *SIAM Journal on Applied Mathematics*, 63:1539–1560, 2003.
- [7] Kyle T Mandli, Aron J Ahmadi, Marsha Berger, Donna Calhoun, David L George, Yiannis Hadjimichael, David I Ketcheson, Grady I Lemoine, and Randall J LeVeque. Clawpack: building an open source ecosystem for solving hyperbolic pdes. *PeerJ Computer Science*, 2:e68, 2016.
- [8] DH Peregrine. Long waves in a uniform channel of arbitrary cross-section. *Journal of fluid mechanics*, 32(2):353–365, 1968.
- [9] Manuel Quezada de Luna and David I. Ketcheson. Two-dimensional wave propagation in layered periodic media. *SIAM Journal on Applied Mathematics*, 74(6):1852–1869, 2014.
- [10] Manuel Quezada de Luna and David I Ketcheson. Solitary water waves created by variations in bathymetry. *Journal of Fluid Mechanics*, 917:A45, 2021.
- [11] Michelle H Teng and Theodore Y Wu. Effects of channel cross-sectional geometry on long wave generation and propagation. *Physics of Fluids*, 9(11):3368–3377, 1997.
- [12] Darryl H Yong and J Kevorkian. Solving boundary-value problems for systems of hyperbolic conservation laws with rapidly varying coefficients. *Studies in Applied Mathematics*, 108(3):259–303, 2002.